Kinetics of Enol Formation from Reaction of OH with Propene

Lam K. Huynh,[†,‡] Hongzhi R. Zhang,[§] Shaowen Zhang,[||] Eric Eddings,[§] Adel Sarofim,[§] Matthew E. Law,[⊥] Phillip R. Westmoreland,[⊥] and Thanh N. Truong*[,‡]

Henry Eyring Center for Theoretical Chemistry, Department of Chemistry, University of Utah, Salt Lake City, Utah 84112, Department of Chemical Engineering, University of Utah, Salt Lake City, Utah 84112, Beijing Institute of Technology, Beijing, China, and Department of Chemical Engineering, University of Massachusetts, Amherst, Massachusetts 01003-9303

Received: September 10, 2008; Revised Manuscript Received: January 26, 2009

Kinetics of enol generation from propene has been predicted in an effort to understand the presence of enols in flames. A potential energy surface for reaction of OH with propene was computed by CCSD(T)/cc-pVDZ//B3LYP/cc-pVTZ calculations. Rate constants of different product channels and branching ratios were then calculated using the Master Equation formulation (*J. Phys. Chem. A* **2006**, *110*, 10528). Of the two enol products, ethenol is dominant over propenol, and its pathway is also the dominant pathway for the OH + propene addition reactions to form bimolecular products. In the temperature range considered, hydrogen abstraction dominated propene + OH consumption by a branching ratio of more than 90%. Calculated rate constants of enol formation were included in the Utah Surrogate Mechanism to model the enol profile in a cyclohexane premixed flame. The extended model shows consistency with experimental data and gives 5% contribution of ethenol formation from OH + propene reaction, the rest coming from ethene + OH.

I. Introduction

Together with theory and experimentation, computational science now constitutes the "third pillar" of scientific inquiry, enabling researchers to understand complex phenomena through their models.[1] In terms of chemical processes, detailed kinetic mechanisms (or models) for hydrocarbon oxidation have played an important role in understanding and reducing pollutant formation in combustion,[2] depicting partial oxidation in solid-oxide fuel cells,[3,4] modeling oxidation in supercritical water,[5] and elucidating the hydrocarbon chemistry in planetary atmospheres.[6] Therefore, there is an essential need that such mechanisms have the ability of capturing all relevant chemistry in such processes. In principle, they should consist of all possible reaction pathways which involve all possible chemical species. However, building such a "complete chemistry" kinetic mechanism a priori is an extremely difficult task because of the very large number of reactions and species that may be involved. Thus, practical mechanisms often rely on the available data (experimental and/or calculated) to limit the number of reactions and species and to provide some forms of validation. Such a practice, however, provides no proof that the mechanism is complete until new chemical species or reactions are observed.

Recently Taatjes et al.[7] used a new flame analysis to detect enols, compounds bearing OH groups adjacent to a carbon−carbon double bond, in a wide range of hydrocarbon flames of both aromatic and aliphatic hydrocarbons. In some flames, enols were found to be present in substantial concentrations, up to 10^{-4} in mole fraction. This discovery suggested that the new species should be incorporated into the existing detailed kinetic mechanisms in order to investigate their practical significance, even though they are minor components in flames. However, little is known about the formation or consumption reactions of gas-phase neutral enols.

In a subsequent study, Taatjes and co-workers[8] provided some initial efforts on understanding enol chemistry by modeling its concentration profile in methane, ethane, ethanol, propene, allene, propyne, and cyclopentene premixed flames using an OH + C_2H_4 reaction from the work of Senosiain et al.[9] as the primary source of enol formation. Although the OH + propene reaction was also included in this study, its kinetic data were only estimated. It is expected that in flames where propene concentration is large, such as in a propene premixed flame,[8] reaction of OH with propene is possibly a substantial source of ethenol. In order to further understand enol chemistry, detailed studies of OH with other alkenes are needed, information on not only the formation but also the consumption of these enol species.

In this study, we have mapped out the detailed potential energy surface (PES) for the OH + propene reaction using an accurate ab initio quantum chemistry method. Both hydrogen abstraction and radical addition reaction channels were considered. This multichannel multiwell PES was used with the Master Equation (ME) methodology[10−12] to provide first-principles-based kinetic information for the ethenol formation channel. This information, with estimations for enol consumption chemistry, was used to model enol formation in a cyclohexane premixed flame. Comparison with experimental data was made to test the mechanism and provide information on the roles of the OH + propene reaction in enol formation.

II. Computational Details

A. Electronic Structure Calculations. A hybrid nonlocal Density Functional Theory (DFT), Becke's gradient-corrected exchange-correlation density functional method (B3LYP)[13] with

* To whom correspondence should be addressed: e-mail, truong@chem.utah.edu.
[†] Current address: Chemical Engineering Department, Colorado School of Mines, Golden, CO 80401.
[‡] Henry Eyring Center for Theoretical Chemistry, Department of Chemistry, University of Utah.
[§] Department of Chemical Engineering, University of Utah.
[||] Beijing Institute of Technology.
[⊥] Department of Chemical Engineering, University of Massachusetts.

10.1021/jp808050j CCC: $40.75
Published on Web 03/09/2009

Dunning's correlation-consistent polarized-valence triple-ζ basis set cc-pVTZ,[14] has been used for locating all stationary points, namely, reactants, transition states, intermediates, and products for the addition reactions. Normal mode analyses were done at the same level of theory for all species. Intrinsic Reaction Coordinate (IRC)[15] calculations were performed to confirm all transition states and their corresponding reactants and products. The energies at all stationary points were then refined at the CCSD(T)/cc-pVDZ level using the B3LYP/cc-pVTZ geometries, which is denoted as CCSD(T)/cc-pVDZ//B3LYP/cc-pVTZ.

Use of Becke's half and-half (BH&H)[16] nonlocal exchange with Lee−Yang−Parr (LYP)[17] nonlocal correlation functionals has been found to be sufficiently accurate for predicting the transition-state properties for hydrogen abstraction reactions by a radical;[18−22] thus, geometries of stationary points for hydrogen abstraction reactions were optimized using this DFT functional with the cc-pVTZ basis set. Single-point energy correction at the CCSD(T)/cc-pVTZ//BH&HLYP/cc-pVTZ level was found to be necessary for accurate rate calculations for this type of reaction. Furthermore, as discussed below the hydrogen abstraction channel contributes more than 90% of the total enol formation from the OH + propene reaction and thus the potential energy surface information needs to be more accurate than that of the addition channel. All electronic structure calculations were carried out using the Gaussian 03 program package.[23]

B. Rate-Constant Calculations. We have employed the Master Equation formulation[10,24] to calculate pressure- and temperature-dependent rate constants for reactions on the multichannel multiwell potential energy surface. Only the main features of our ME implementation are briefly presented here. More details and test cases can be found in a future publication.[25]

In this study, we employed a one-dimensional (1-D) Master Equation in which the total rovibrational energy, E, is the independent variable. There are three main assumptions in the ME formulation: (i) the reactants maintain a thermal distribution with the bath gas throughout the course of the reaction; (ii) the number density of bath gas molecules is much larger than those of reactants, and if there are two reactants, then the number density of one is much larger than that of the other; and (iii) any bimolecular product channel is treated as an "infinite sink"; i.e., once the dissociation products are formed, they will never return to the wells. The second assumption makes any bimolecular reaction pseudo first order. The rate constants were computed as functions of pressure and temperature by solving the total-energy-resolved master equation for a system with M wells

$$\frac{dn_i(E)}{dt} = Z\int_{E_{0i}}^{\infty} P_i(E,E')n_i(E')\,dE' - Zn_i(E) - \sum_{j\neq i}^{M} k_{ji}(E)n_i(E) + \sum_{j\neq i}^{M} k_{ij}(E)n_j(E) - k_{di}(E)n_i(E)\delta_{id} + K_{eqi}k_{di}(E)F_i(E)n_R n_m\delta_{id} - \sum_{p=1}^{N_p} k_{pi}(E)n_i(E)\delta_{pi} \quad (1)$$

$$i = 1, ..., M$$

where t is the time; E is the total internal energy; Z is the collision number per unit time, which is assumed to be the Lennard-Jones collision rate, Z_{LJ}; $n_i(E)\,dE$ is the number density of molecules (or complexes) in the ith well with energy between E and $E + dE$; E_{0i} is the ground-state energy for the ith well; M is the number of wells; $P_i(E,E')$ is the probability that a molecule in the ith well with energy between E' and $E' + dE'$ will be transferred by collision to a state with energy between E and $E + dE$; $k_{ij}(E)$ is the microcanonical (RRKM) rate constant for isomerization from the jth well to the ith well; $k_{di}(E)$ and $k_{pi}(E)$ are the microcanonical rate constants for dissociation from the ith well to reactants and products, respectively; n_R and n_m are the number densities of the two reactants (OH and $CH_3CH{=}CH_2$, respectively, as in this present case); K_{eqi} is the equilibrium constant for the association reaction between the reactants and the intermediate designated as the ith well; and N_P is the number of bimolecular product channels. We have included the Kronecker delta δ_{id} and δ_{pi} to take into account whether the ith well is formed directly from reactants and dissociates to form products, respectively.

The function $F_i(E)$ is the equilibrium energy distribution in the ith well at temperature T

$$F_i(E) = \rho_i(E)e^{-E/k_B T}/Q_i(T) \quad (2)$$

where $\rho_i(E)$is the density of states of the ith well, $Q_i(T)$is its partition function, and k_B is the Boltzmann's constant. As mentioned above, if the reaction is bimolecular, it can be treated as a pseudo-first-order (unimolecular) reaction. The change of population of the reactant R can be expressed as

$$\frac{dn_R}{dt} = \sum_{i=1}^{M}\int_{E_{0i}}^{\infty} k_{di}(E)n_i(E)\delta_{id}\,dE - n_R n_m\sum_{i=1}^{M} K_{eqi}\int_{E_{0i}}^{\infty} k_{di}(E)F_i(E)\delta_{id}\,dE \quad (3)$$

The detailed-balance condition is used for the relation between $P(E,E')$ and $P(E',E)$ as well as for the relation between $k_{ij}(E)$ and $k_{ji}(E)$

$$P_i(E',E)F_i(E) = P_i(E,E')F_i(E') \quad (4)$$

$$k_{ij}(E)\rho_j(E) = k_{ji}(E)\rho_i(E) \quad (5)$$

The function $P(E,E')$ is the probability that a complex with energy between E' and $E' + dE'$ will be transferred by a collision to a state with energy between E and $E + dE$. It is approximated here by a single-exponential down function[26]

$$P(E,E') = \frac{1}{C_N(E')}\exp\left(-\frac{E'-E}{\langle\Delta E_d\rangle}\right) \quad (6)$$

$$E'>E$$

where $C_N(E')$ is the normalization constant and $\langle\Delta E_d\rangle$ is the averaged energy transferred in a deactivating collision, which depends on the nature of the colliding gas as a function of temperature and, in some cases, of energy.

Collision rate Z_{LJ} can be calculated using Lennard-Jones potential parameters as

$$Z = Z_{\text{hard-sphere}}\Omega \quad (7)$$

where $Z_{\text{hard-sphere}}$ is the hard-sphere collision rate derived from the elementary gas-phase kinetic theory and Ω is a dimensionless collision integral calculated by the expression given in Reid et al.[27] The discussion about this expression/formulation can be found elsewhere.[12]

The ME methodology requires a microcanonical rate constant $k(E)$ in the case of the 1-D ME, for each isomerization and dissociation/association process involved in the overall reaction. These rate constants can be calculated using the RRKM theory. Detailed discussion on calculations of $k(E)$ can be found elsewhere.[12,28] A number of elementary unimolecular reactions involve migration of hydrogen atoms, and thus tunneling effects on microcanonical rate constants[29] were expected to be large. Therefore, the inclusion of these effects was taken into account for these reactions.

In this study, eqs 1 and 3 were integrated directly with time using an ordinary differential equation(ODE) solver[10,30,31] after representing the integrals in these equations as discrete sums using a simple rectangular rule with grid spacing dE (the energy step in this study). The populations of species as functions of time can be obtained directly and first-order rate constants can be extracted from the reactant population using the "exponential decay" approach. Solving the ME by direct integration is more time-consuming than the eigenvalue analysis approach; however, it is known to be more stable and robust.[32] In this study, we limit our focus on one product channel, namely, the enol formation. Performance and accuracy of the general ME method will be presented in ref 25.

For ME calculations, experimental conditions for the cyclohexane premixed flame of Law et al.[29] were used to facilitate comparisons, namely, Ar bath gas at 30 Torr. The Lennard-Jones parameters for all intermediates (C_3H_7O) were estimated using the parameters for C_3H_6OH.[33] It is known that the energy-transfer parameter depends on temperature and on the nature of the bath gas. Calculations also require a value for $\langle \Delta E_d \rangle$, the average energy transferred in a deactivating collision between these partners. We found that calculated rate constants for this reaction are relatively insensitive to the value of $\langle \Delta E_d \rangle$ over the range of temperatures considered here. Particularly, the use of $\langle \Delta E_d \rangle = 200\ \text{cm}^{-1}(T/298\ \text{K})^{0.85}$ for complexes of the OH + C_2H_4 system,[9] $\langle \Delta E_d \rangle = 300\ \text{cm}^{-1}$ for OH + CH_2=CHCH=CH_2 system[34] as well as other different temperature-independent $\langle \Delta E_d \rangle$ values (from 200 to 500 cm^{-1}) gives similar rate constants (the difference is less than 1%) for the ethenol channel (channel **P3** in Figure 3). Therefore, for simplicity, the value of $\langle \Delta E_d \rangle = 200\ \text{cm}^{-1}$ was used for all complexes in the temperature range of 400−2500 K. An energy step (or energy grain) of 100 cm^{-1} was used except for the cases at high temperatures (>1000 K), where an energy step of 200 cm^{-1} was used instead.

We also considered the spin−orbit interaction for OH radical in its electronic partition function by including both the $^2\Pi_{3/2}$ and the ground-state $^2\Pi_{1/2}$ levels. The splitting of 126 cm^{-1} between these levels was used.[11] Similarly to the previous study[9] of the reaction of OH with ethylene, we ignored this effect at the transition state because it is expected to be small.

Rate constants of the hydrogen abstraction reactions were calculated using the canonical transition state theory (TST)[35] with the Eckart tunneling correction[36] (denoted as TST/Eckart). All TST/Eckart calculations were carried out using the TheRate module of the Computational Science and Engineering Online (CSE-Online) cyber-environment.[37]

C. Premixed Flame Simulations. The package CHEMKIN IV[38] was used to simulate the laminar premixed flat flame with the Utah Surrogate Kinetic Model.[39] The mechanism consists of about 30 submechanisms of various chemical compounds and has been validated with 41 flames, including *n*-heptane, *n*-decane, *n*-hexadecane, kerosene, and synthetic gas. More detailed information on this kinetic model is available elsewhere.[40]

III. Results and Discussion

A. OH + CH_3CH=CH_2 Potential Energy Surface. The potential energy surface is rather complex for the reaction of OH radical with propene (referred to as C_3H_7O PES), including all possible elementary reactions for association/dissociation, abstraction, and isomerization reactions that eventually lead to bimolecular products, is presented in Figure 1 with all possible stationary points (reactants, intermediates, transition states, and products). More detailed information for stationary points on the PES is given in Table 1. The optimized geometries as well as the corresponding frequencies can be found in the Supporting Information. Note that all energies discussed hereafter are zero-point-corrected values relative to that of the reactants unless otherwise indicated. Also in the construction of this PES, if there is more than one possible conformer for a given structure, the lowest-energy conformer is used. The PES for the OH addition to propene consists of 8 intermediates (denoted as "**I**"), 22 transition states ("**TS**"), and 8 bimolecular products channels ("**P**"). These product channels are **P1** (acetaldehyde channel, CH_3CHO + •CH_3), **P2** (acetone channel, CH_3COCH_3 + •H), **P3** (ethenol channel, CH_2=CHOH + •CH_3), **P4** (2-propenol channel $CH_3C(OH)$=CH_2 + •H), **P5** (3-propenel channel, CH_2=$CHCH_2OH$ + •H), **P6** (1-propenol channel, CH_3CH=CHOH + •H), **P7** (propanal channel, CH_3CH_2CHO + •H), and **P8** (formaldehyde channel, HCHO + •C_2H_3). Intermediates also referred to as "wells" are the adduct complex **C** (HO···CH_2=$CHCH_3$), **I1** ($CH_3CHOHCH_2$•), **I2** (CH_3CHO•CH_3), **I3** (CH_3C•$OHCH_3$), **I4** (CH_3C•HCH_2OH), **I5** ($CH_3CH_2CH_2O$•), **I6** (•$CH_2CH_2CH_2OH$), and **I7** (CH_3CH_2C•HOH). The notation "**TS_I*a*−I*b***" means that the transition state connects intermediate **Ia** and intermediate **Ib**, where *a* and *b* are integer numbers. The dot sign "•" denotes the location of a radical.

For the addition reactions, OH radical first may form a van der Waals complex (**C**) with propene before it inserts into the C−C double bond to form either the intermediate **I1** (nonterminal addition) or **I4** (terminal-carbon addition). The optimized geometrical parameters of the complex **C**, together with those recently reported by Szori et al.[21] at the CCSD/6-31G(d) level, are given in Figure 2. It is found that the optimized geometrical parameters for B3LYP (the present study) are close to those from the CCSD calculations. Because this complex is not critical to the overall reaction in the combustion regime ($T > 500$ K), we will not discuss it further.

To form the adduct **I1** or **I4**, the complex **C** must pass over the transition states **TS_C−I1** or **TS_C−I4** with a barrier of 1.5 kcal/mol. From the **I1** and **I4** intermediates, the system undergoes isomerization processes to form several intermediates (**I2** and **I3** from**I1**; **I5**−**I7** from **I4**) and eventually exits by a number of bimolecular product channels, namely, four product channels (**P1**−**P4**) from **I1** and five (**P3**, **P5**−**P8**) from **I4**. It is noted that the intermediates **I1**, **I2**, and **I3** can interconvert, as do the intermediates **I4**, **I5**, **I6**, and **I7**. Of the eight product channels, the most thermodynamically favored one is **P1** for forming CH_3CHO + •CH_3, while the least favorable is **P5** for producing CH_2=$CHCH_2OH$ + •H. This study focuses on the ethenol formation, the product channel**P3**; thus, all reaction paths from **I1** and **I4** leading to these products are summarized in Figure 3.

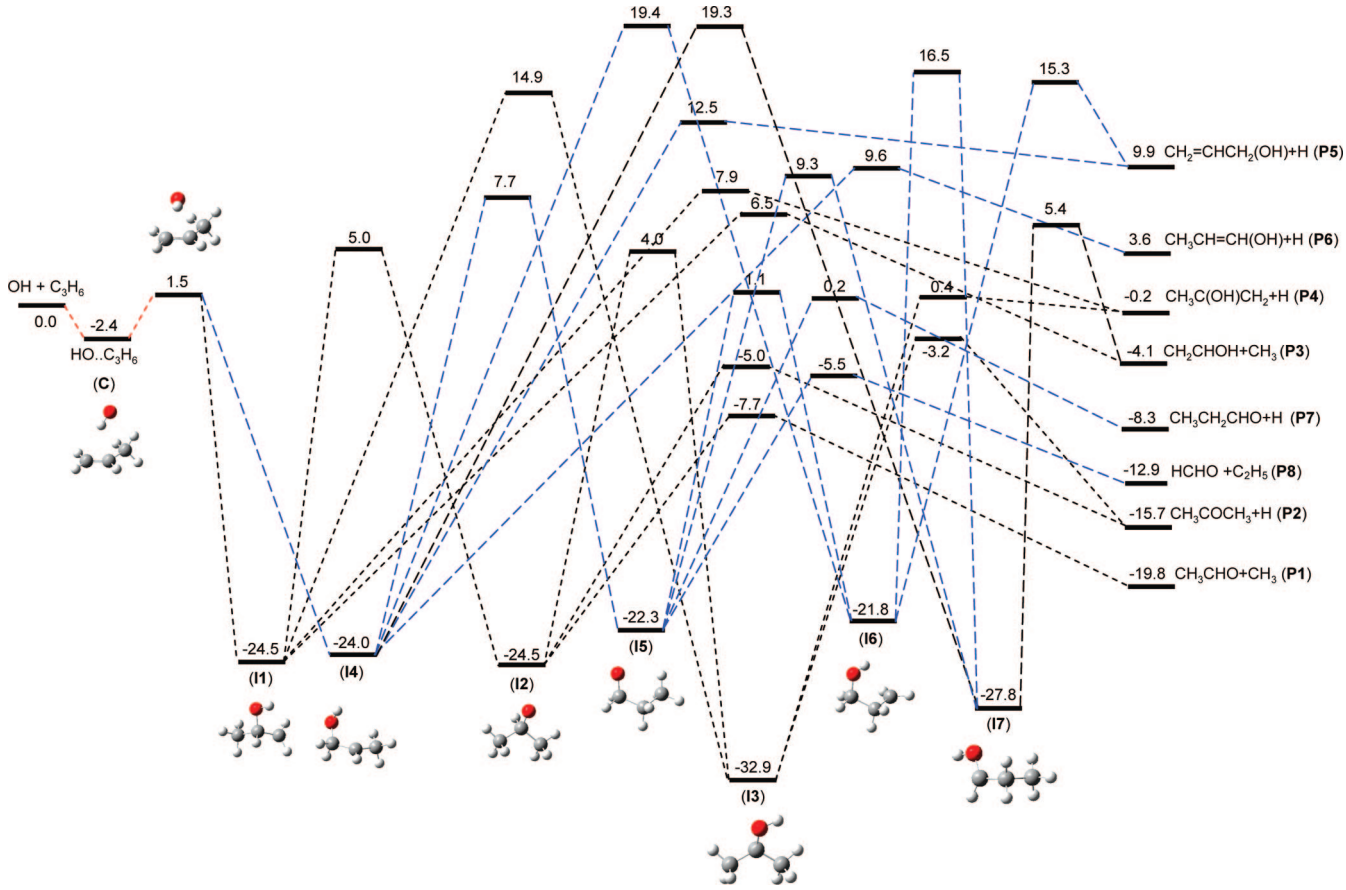

Figure 1. OH + C_3H_6 (C_3H_7O) classical potential energy surface for the addition reactions leading to bimolecular products at the CCSD(T)/cc-pVDZ//B3LYP/cc-pVTZ level of theory. The number is the energy in kcal/mol relative to that of the reactants. Zero-point-energy-corrected relative energies at stationary points are given.

Formation of the products **P3** (ethenol + CH_3) is exothermic with the zero-point-energy-corrected reaction energy of 4.1 kcal/mol below that of the separated reactants. Ethenol can be formed from two parallel channels. One channel is from the intermediate **I1** via the β-scission reaction of the C−C bond with a barrier height of 6.5 kcal/mol above the combined reactant energy. Note that **I1** can isomerize to form the intermediate **I2** and **I3** through 1,3 and 1,2 hydrogen migration reactions, respectively. However, **I2** and **I3** do not lead to enol formation. Enol also can be formed directly from the intermediate **I1**. The other enol formation channel is from the intermediate **I4**, which can isomerize to form the intermediates **I5**, **I6**, and **I7** by hydrogen migration reactions having rather high barriers. Ethenol is formed from the C−C bond cleavage of the intermediate **I7** with a barrier of 5.4 kcal/mol.

Competing with the OH + propene addition reactions are the hydrogen abstraction reactions by OH radical. Propene has three distinct hydrogen atom types and thus has three possible abstraction reactions. The first two reactions form propenyl-1 ($CH_3CH{=}CH\bullet$) and propenyl-2 ($CH_3C\bullet{=}CH_2$) radicals with barriers of 4.6 and 3.2 kcal/mol, respectively. The third one has a lower barrier of 1.6 kcal/mol due to formation of a resonant radical, allyl ($\bullet CH_2CH{=}CH_2$). Rate constants for these reactions were calculated using the energetic information given in Table 1.

B. Rate Constant Calculations. ***B.1. Addition Reactions to Form Bimolecular Products.*** Because product formation in the high temperature range is of interest in this study, we primarily focus on the rate constants of addition reactions to form bimolecular products, not those reactions that form intermediates such as **I1** and **I4**. In the temperature range of 500−2500 K, such addition reactions to form intermediates are assumed unimportant to the overall kinetics,[41] and the contribution of the van de Waals complex C is also expected to be insignificant. Thus, more rigorous treatment, such as the two-transition-state model which was used to study the addition of OH with ethylene, is not needed.[9]

Rate constants for bimolecular product formation were evaluated at the half-life time of the reactants using the "exponential decay" approach.[10] Results for ethenol formation are discussed in detail here, while rate constants for other product channels are mentioned only as an extension of the discussion:

For ethenol formation at temperatures lower than 400 K, formation of the thermalized intermediates **I1** and **I4** is dominant. In other words, more than 99% of the population of reacted reactants is trapped in these two wells. The rate constant for the ethenol formation is consequently very small.

As temperature increases above 400 K, ethenol formation becomes noticeable. When temperature is in the range of 400−450 K, the product channels are a mixture of ethenol and **I3** formation. This result means that populations of high-energy states of **I1** and **I4** transform rapidly to **I3** and the products **P3**. Therefore the consumption rate of reactants is the sum of rates for **I3** and ethenol formation. The ratio of **P3**/**I3** formation is about 2.0 at 400 K and rapidly increases to 1000 at 450 K.

At temperatures higher than 450 K, the population of thermalized intermediate **I3** is insignificant (around 10^{-6} times smaller) compared to that of ethenol. Thus, the rate constants for ethenol formation can be obtained directly from the

TABLE 1: Classical, Zero-Point Energies and Zero-Point-Corrected Energies of Reactants, Transition States, and Bimolecular Products (Energies in kcal/mol)

species	classical energy[a]	zero-point energy (ZPE)[b]	ZPE-corrected energy[c]	species	classical energy[a]	zero-point energy (ZPE)[b]	ZPE-corrected energy[c]
			Addition Channels				
Reactants	0.0	0.0	0.0				
C	−3.7	1.3	−2.4	**TS_I1−P4**	8.8	−0.9	7.9
I1	−27.7	3.2	−24.5	**TS_I2−P1**	−8.7	1.0	−7.7
I2	−28.0	3.5	−24.5	**TS_I2−P2**	−3.6	−1.4	−5.0
I3	−36.6	3.7	−32.9	**TS_I3−P2**	−1.1	−2.1	−3.2
I4	−27.5	3.5	−24.0	**TS_I3−P4**	2.2	−1.8	0.4
I5	−25.7	3.4	−22.3	**TS_I4−P5**	13.9	−1.4	12.5
I6	−25.3	3.5	−21.8	**TS−I4-P6**	10.6	−1.0	9.6
I7	−32.0	4.2	−27.8	**TS_I5−P7**	1.6	−1.4	0.2
TS_C−I1/-I4	−0.2	1.7	1.5	**TS_I5−P8**	−6.9	1.4	−5.5
TS_I1−I2	4.1	0.9	5.0	**TS_I6−P5**	16.3	−1.0	15.3
TS_I1−I3	14.5	0.4	14.9	**TS_I7−P3**	4.6	0.8	5.4
TS_I2−I3	3.3	0.7	4.0	**P1**	−18.0	−1.8	−19.8
TS_I4−I5	6.4	1.3	7.7	**P2**	−12.8	−2.9	−15.7
TS_I4−I6	18.3	1.1	19.4	**P3**	−2.8	−1.3	−4.1
TS_I4−I7	18.7	0.6	19.3	**P4**	1.9	−2.1	−0.2
TS_I5−I6	−0.5	1.6	1.1	**P5**	11.8	−1.9	9.9
TS_I5−I7	8.2	1.1	9.3	**P6**	5.7	−2.1	3.6
TS_I6−I7	15.7	0.8	16.5	**P7**	−5.9	−2.4	−8.3
TS_I1−P3	5.7	0.8	6.5	**P8**	−11.5	−1.4	−12.9
			Abstraction Channel[d]				
TS_CH_3CHCH	6.5	−1.9	4.6	**$CH_3CHCH + H_2O$**	−4.5	−0.6	−5.1
TS_CH_3CCH_2	5.3	−2.0	3.3	**$CH_3CCH_2 + H_2O$**	−7.9	−0.7	−8.6
TS_CH_2CHCH_2	3.1	−1.5	1.6	**$CH_2CHCH_2 + H_2O$**	−27.9	−0.5	−28.4

[a] Calculated at CCSD(T)/cc-pVDZ//B3LYP/cc-pVTZ. [b] Calculated using the B3LYP/cc-pVTZ frequencies with no scaling factor introduced. [c] Sum of the columns 2 and 3. [d] The same as the addition reaction but the geometries and frequencies are at BH&HLYP/cc-pVTZ and the energies are at CCSD(T)/cc-pVTZ//BH&HLYP/cc-pVTZ. Product channels: **P1** ($CH_3CHO + \bullet CH_3$), **P2** ($CH_3COCH_3 + \bullet H$), **P3** ($CH_2{=}CHOH + \bullet CH_3$), **P4** ($CH_3COH{=}CH_2 + \bullet H$), **P5** ($CH_2{=}CHCH_2OH + \bullet H$), **P6** ($CH_3CH{=}CHOH + \bullet H$), **P7** ($CH_3CH_2CHO + \bullet H$), and **P8** ($HCHO + \bullet C_2H_5$).

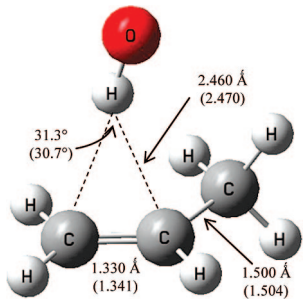

Figure 2. The optimized geometry of the van der Waals complex **C**. The numbers in parentheses are at CCSD/6-31G(d) level from ref 21.

exponential decay of the reactant concentration for $T > 450$ K. Rate constants for ethenol formation calculated in the temperature range of 500−2500 K are plotted in Figure 4 and fitted to a van Kooij form as

$$k(T) = (1.33 \times 10^{-18})T^{2.073} \exp\left[-\frac{3010}{T}\right], \text{cm}^3\ \text{molecule}^{-1}\ \text{s}^{-1} \quad (8)$$

The calculated rate constants show strong, non-Arrhenius temperature dependence. A previously estimated, single-value rate constant for this reaction, obtained by fitting the ethenol concentration profile in a propene premixed flame, is within an order of magnitude compared to our computed results in the temperature range of 1000−2000 K.[8]

As mentioned earlier, there are two channels contributing to the ethenol formation. The first one is from intermediate **I1**, and the second channel is from intermediate **I4**. Rate constants for each channel as well as the ratio between the two at several selected temperatures are given in Table 2. The overall rate constants of ethenol formation are also given. It can be seen that the first channel is dominant for the whole temperature range. This result can be explained by the much lower reaction barrier from **I1** to the products, 6.5 kcal/mol (see Table 1 and Figure 3), while the second channel has higher barriers (**TS_I4−I5**, **TS_I4−I6**, **TS_I4−I7**, **TS_I5−I6**, **TS_I6−I7**) of up to 20 kcal/mol. When temperature increases, the contribution of the second channel increases (see Table 2) but still has a minor contribution to ethenol formation (less than 3% at 2500 K).

We also calculated the rate constants for all bimolecular product channels presented in Figure 1. The calculated rate constants for each product channel were fitted to van Kooij forms and are given in Table 3. The product distribution obtained from these rate constants in the temperature range of 500−2500 K is given in Figure 5. The ethenol formation **P3** channel is not the most thermodynamically stable one, as it has a relative energy of −4.1 kcal/mol compared to −19.8 kcal/mol for the most stable channel **P1**, $CH_2CHO + CH_3$. However, it is kinetically the most favored exit channel for the addition of OH to propene because of the difference in the barrier heights. As shown in Figure 5, at 500 K, ∼48% of the reacting population transforms into the products ethenol and methyl radical. As temperature increases, the contribution of this channel reaches a peak of 75% at ∼1100 K and decreases gradually as contributions from other channels increase. The other product channels have different trends. The branching ratios to channels **P1**, **P2**, and **P4** decrease as temperature increases and level off in the high-temperature range, while those

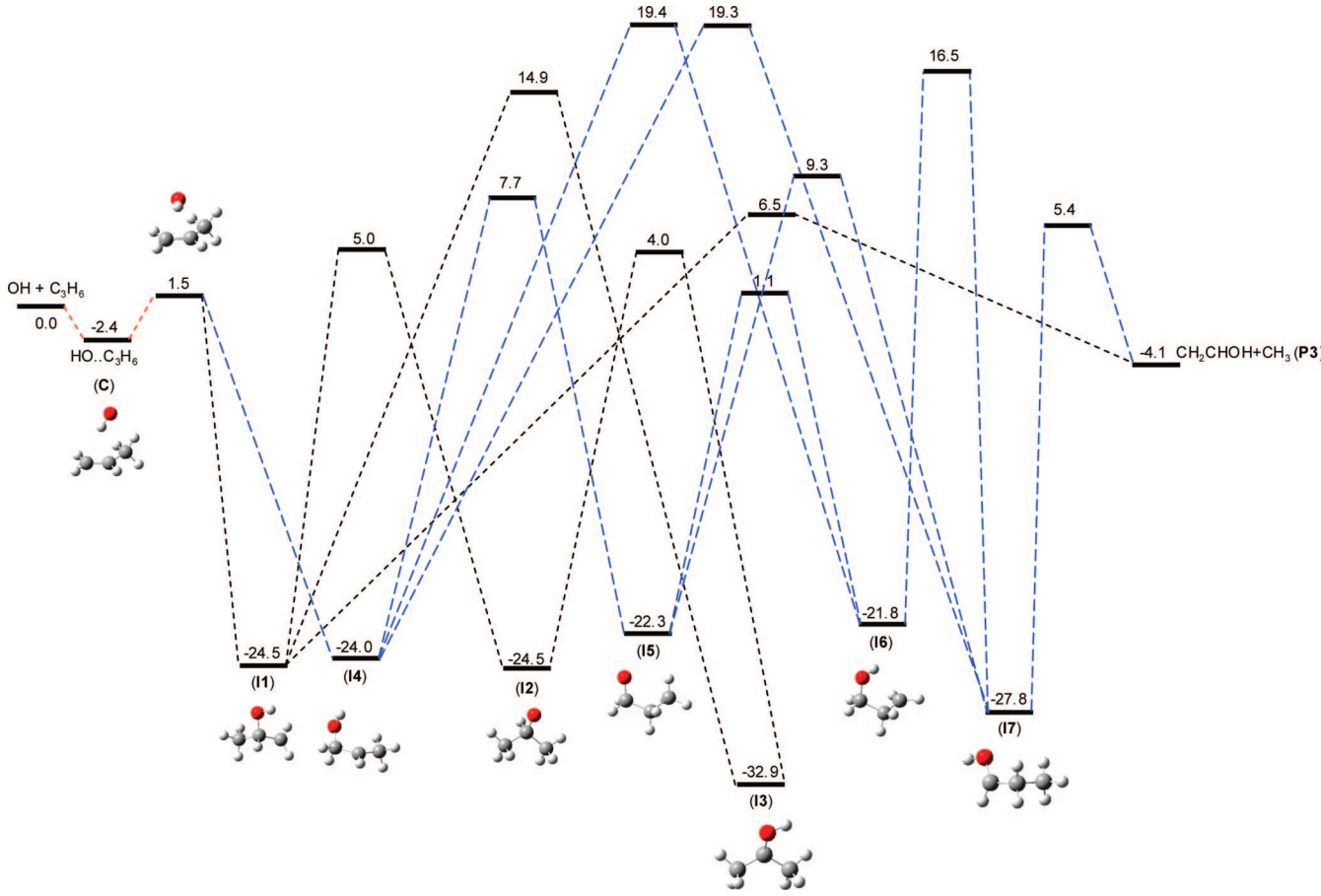

Figure 3. Similar to Figure 1 but specifically for the ethenol formation. The short-dashed line is the pathway starting from intermediate **I1** and the long-dashed one from intermediate **I4**.

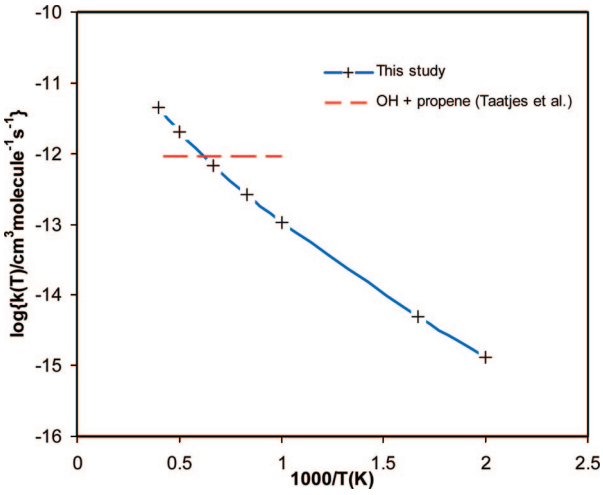

Figure 4. Arrhenius plot of rate constants of ethenol formation from the reaction of OH with propene in the temperature range of 500−2500 K.

to channels **P5** and **P6** increase with the temperature. The contributions from channels **P7** and **P8** are less than 2% even at high temperatures. Note that the thermalized adducts and isomers are never significant at the low pressure examined, and only bimolecular products result.

It is worthwhile also to discuss formation of the other enol, propenol. Propenol can be formed by C−H fission from the OH + propene adduct. If an OH radical attaches to the terminal carbon of the double bond, the product 2-propenol (**P4**) is formed; otherwise 1-propenol (P6) is formed. It can be seen that 2-propenol (**P4**) is preferred at low temperatures, while more

TABLE 2: Rate Constants for Two Different Ethenol Formation Channels at Different Temperatures[a]

temp (K)	$k^{\text{channel-I}}$	$k^{\text{channel-II}}$	$k^{\text{channel-I}}/k^{\text{channel-II}}$	k^{Total}
500	1.29×10^{-15}	$4.93 \times ^{-18}$	261	$1.29 \times ^{-15}$
600	$4.99 \times ^{-15}$	$2.24 \times ^{-17}$	223	$5.02 \times ^{-15}$
800	$3.14 \times ^{-14}$	$1.64 \times ^{-16}$	192	$3.16 \times ^{-14}$
1000	$1.07 \times ^{-13}$	$6.18 \times ^{-16}$	173	$1.08 \times ^{-13}$
1500	$6.80 \times ^{-13}$	$6.02 \times ^{-15}$	113	$6.86 \times ^{-13}$
2000	$2.03 \times ^{-12}$	$3.07 \times ^{-14}$	66	$2.06 \times ^{-12}$
2500	$4.32 \times ^{-12}$	$1.04 \times ^{-13}$	42	$4.43 \times ^{-12}$

[a] Units are cm^3 $molecule^{-1}$ s^{-1}.

TABLE 3: Fitted Parameters[a] for Calculated Rate Constants

product channel	A	n	E_a/R
P1($CH_3CHO + \bullet CH_3$)	$1.19 \times ^{-22}$	2.793	$1.02 \times ^{+3}$
P2($CH_3COCH_3 + \bullet H$)	$8.57 \times ^{-23}$	2.832	$9.71 \times ^{+2}$
P3 ($CH_2{=}CHOH + \bullet CH_3$)	$1.33 \times ^{-18}$	2.073	$3.01 \times ^{+3}$
P4($CH_3COH{=}CH_2 + \bullet H$)	$9.36 \times ^{-26}$	3.739	$6.40 \times ^{+2}$
P5($CH_2{=}CHCH_2OH + \bullet H$)	$8.46 \times ^{-21}$	2.622	$5.83 \times ^{+3}$
P6($CH_3CH{=}CHOH + \bullet H$)	$2.18 \times ^{-21}$	2.698	$4.11 \times ^{+3}$
P7 ($CH_3CH_2CHO + \bullet H$)	$3.50 \times ^{-26}$	3.741	$1.62 \times ^{+3}$
P8 ($HCHO + \bullet C_2H_3$)	$2.72 \times ^{-26}$	3.775	$1.60 \times ^{+3}$
total	$3.49 \times ^{-21}$	2.838	$2.05 \times ^{+3}$

[a] $k(T) = A\ T^n \exp(-E_a/RT)$, cm^3 $molecule^{-1}$ s^{-1}. Temperature is in kelvins (K).

1-propenol is produced at high temperatures (see Figure 5). This result can be explained by the lower barrier of the 2-propenol channel. (Note that there are two parallel channels leading to the formation of 2-propenol, one from the intermediate **I1** and

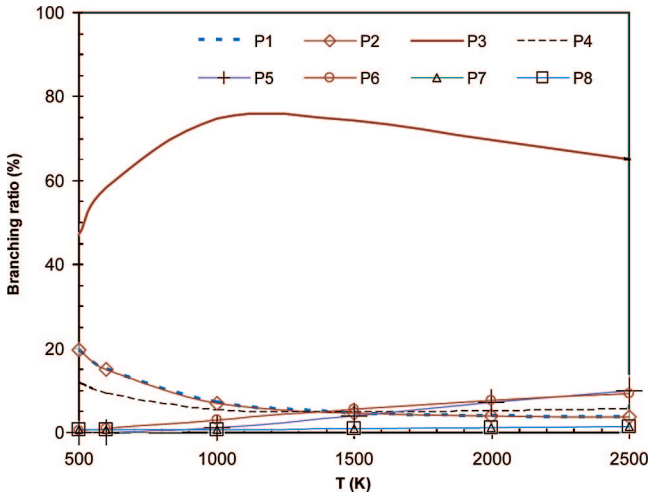

Figure 5. Product branching fractions at 30 Torr of Ar bath gas. Product channels are **P1** ($CH_3CHO + \bullet CH_3$), **P2** ($CH_3COCH_3 + \bullet CH_3$), **P3** ($CH_2{=}CHOH + \bullet CH_3$), **P4** ($CH_3COH{=}CH_2 + \bullet H$), **P5** ($CH_2{=}CH\text{-}CH_2OH + \bullet H$), **P6** ($CH_3CH{=}CHOH + \bullet H$), **P7** ($CH_3CH_2CHO + \bullet H$), and **P8** ($HCHO + \bullet C_2H_3$).

the other from **I3**, while there is only one for 1-propenol.) It can be seen in Figure 5 that ethenol is formed faster than propenol (1-propenol and 2-propenol) in the considered temperature range.

The computed propenol:ethenol ratio is in excellent agreement with the available experimental data. Using mass spectrometry to study the overall kinetics of OH + propene reactions, Hoyermann and Sievert[42] reported the branching ratio of C_2H_4O to C_3H_6O to be about 1:3.5 at room temperature (Taatjes and co-workers[8] later reasoned that C_2H_4O and C_3H_6O are possibly enols), while our calculations give 1:3.8 at 500 K. Moreover, the calculated ratio of propenol to ethenol is around 1:(4 to 7), while the experimental mole fraction ratio was about 1:5 in the flame zone of a rich propene premixed flame ($\phi = 2.3$).[8] Although the comparisons between our calculated branching ratios are in good agreement with experimental data, it should be noted that our calculated ratio is from the single reaction of OH with propene, while the experimental mole fraction ratio is from different reactions in a premixed flame. However, because the propene concentration in propene flames is much larger than those of ethene and butadiene (other enol precursors), one can expect that the OH + propene reaction might be dominant.

B.2. Hydrogen Abstraction and Overall Reactions. In order to obtain the overall rate of the OH + propene reaction, hydrogen abstraction by OH radical must also be included. Rate constants were calculated for hydrogen abstraction at the three sites of propene, yielding propenyl-1, propenyl-2, and allyl radicals using TST with the Eckart tunneling correction. We found that for the hydrogen abstraction reactions, the energetic information should be corrected using single-point energy calculations at the CCSD(T)/cc-pVTZ level of theory in order to obtain accurate results compared to available data in the literature for each site.[41]

The total overall rate constants of the OH + propene reaction are plotted in Figure 6, including available experimental data. Smith et al.[43] used the laser pyrolysis/laser-induced fluorescence (LP-LIF) technique to measure total rate constants at four temperatures in the range of 960−1210 K. Using the same technique, Tully and Goldsmith[44] reported a high-pressure limit expression in the temperature range of 700−896 K. Bott et al.[45] performed shock-tube experiments and recommended values of a factor of 1.8 larger than those of Smith et al. or the

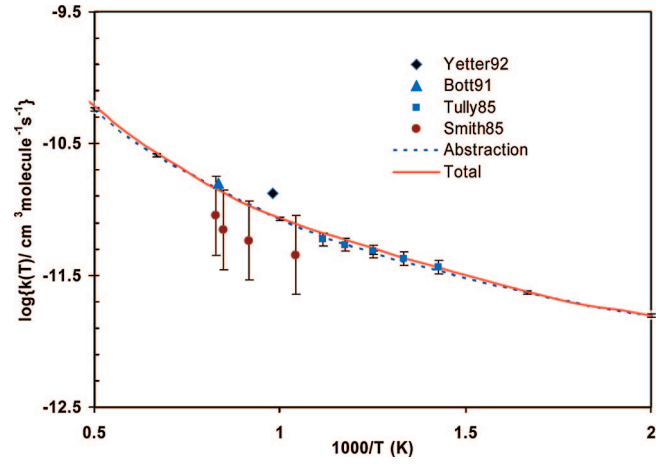

Figure 6. Arrhenius plot of rate constants of abstraction reaction and overall reaction (abstraction and addition reaction to form bimolecular products) of OH with propene in the temperature range of 500−2500 K.

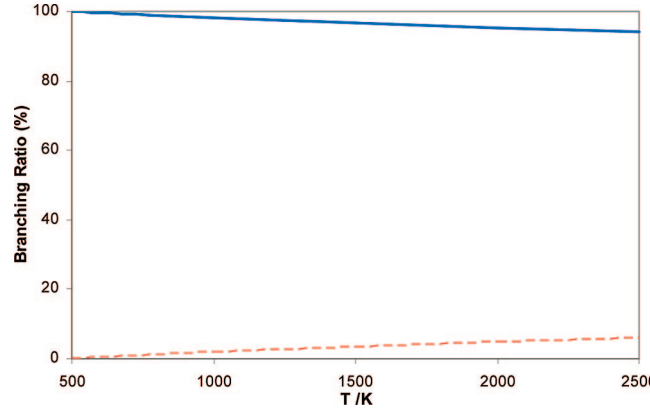

Figure 7. Product branching fractions of abstraction channels and addition channels to form bimolecular products at 30 Torr of Ar bath gas. The solid line is for abstraction reactions; dashed line for addition reactions to form bimolecular products.

extrapolation of Tully and Goldsmith's expression. Yetter et al.[46] derived a higher rate constant at 1020 K that they reasoned might be due to the uncertain contribution of the addition reaction. The present predicted values are within the uncertainty of these experimental data[43−46] in the temperature range of 700−1200 K.

Branching ratio is shown in Figure 7 for the hydrogen abstraction reactions and the addition reactions in the temperature range of 500−2500 K. Abstraction is the dominant reaction pathway, contributing more than 93% reactant consumption for the temperature higher than 500 K. When the temperature increases, the contribution of the abstraction reactions gradually decreases, while that of the addition reactions slightly increases to a maximum of 7% at 2500 K. Addition routes are thus minor routes and thus further improvement on the potential energy surface information for these channels would not change the overall conclusion of this study.

C. Simulation of Enol−Keto Formation. To validate and determine the relative importance of the OH + propene reaction for ethenol formation, the present kinetics for this ethenol formation reaction were added to the Utah Surrogate Mechanism[39] to model a stoichiometric cyclohexane premixed flame at 30 Torr. The calculated rate constants for hydrogen abstractions at propene are also included in the model. Detailed modeling results are presented in a separate publication.[40]

TABLE 4: Contribution of Several Important Reactions to the Ethenol Formation[a]

	reaction	contribution (%)
R1:	$C_2H_4 + OH = C_2H_3OH + H$	78
R2:	$C_3H_6 + OH = C_2H_3OH + CH_3$	5
R3:	$CH_2CHCHCH_2 + OH = C_2H_3OH + C_2H_3$	17
R4:	$C_2H_3OH = CH_3CHO$	~0
R5:	$C_2H_3OH + H = CH_3CHO + H$	68
R6:	$C_2H_3OH + H = CH_2CHO + H_2$	18
R7:	$C_2H_3OH + OH = CH_2CHO + H_2O$	10
R8:	$C_2H_3OH + O = CH_2CHO + OH$	2

[a] The flux analysis was carried out at the maximum concentration of ethenol of a distance of about 1.2 cm above the burner surface.

Addition reactions that were added to the Utah Surrogate Mechanism are summarized in Table 4. Three OH addition pathways were included for the formation of ethenol (**R1**−**R3**), including the reactions with ethene (**R1**), propene (**R2**), and butadiene (**R3**). Senosiain and co-workers[9] proposed a rate constant for OH addition to ethene followed by dehydrogenation (**R1**); the rate constant for **R2** was calculated in this work, and the rate constant for **R3** was estimated by Zhang and co-workers.[40] Ethenol consumption includes hydrogen abstraction of the three chemically different hydrogens and keto−enol tautomerization to form the aldehyde via direct or radical-catalyzed reactions. The unimolecular tautomerization from enol to keto structure (**R4**) requires a 1−3 hydrogen migration with a high barrier, which results in a negligible contribution for the overall tautomerization rate. The isomerization route catalyzed by H (**R5**) is also included for the enol tautomerization. The rate was estimated to be close to that of the H addition to C_2H_4, with the assumption that the leaving of the alcoholic hydrogen is instantaneous. The hydrogen abstraction rates of enol by H (**R6**), OH (**R7**), and O (**R8**) radicals were estimated after examining reference reactions of methanol.[47]

Table 4 shows the contributions of several reactions to ethenol formation at the maximum concentration of ethenol. OH addition to ethylene is the dominant ethenol formation pathway. For example, 78% of the ethenol formation at 1.2 cm above the burner surface, where its concentration reaches the maximum, is from this reaction. The second major pathway is predicted to be the reaction with butadiene (17%), followed by that of propene (5%). Hydrogen-catalyzed tautomerization dominates ethenol consumption (**R5**, 68%) compared to the hydrogen abstraction reactions: 18% from **R6**, 10% from **R7**, and 2% from **R8**. Radical-catalyzed tautomerization was found to be the major formation pathway for acetaldehyde, the keto form of ethenol (45% of the total formation rate), followed by OH combination with vinyl radical (33%, $C_2H_3 + OH = CH_3CHO$) and the addition of O radical to 1-butene (19%, $CH_2CHCH_2CH_3 + O = CH_3CHO + C_2H_4$).

The Utah Surrogate Mechanism also includes reactions that involve C_3 and C_4 enol and aldehyde species using a generic rate approach with rates adjusted for possible resonant structures, different symmetric factors, and other kinetic considerations. The predicted enol and keto concentrations for C_2−C_4 species reproduce the experimental data very well within the experimental uncertainties, as seen in Figure 8.

We have attempted to determine how sensitive ethenol formation is to the rate constant of the reaction R2. If the calculated rate constant is doubled, the contribution from R2 goes up to 10%. This sensitivity means that accuracy in the rate constant's determination is important for predicting enol formation. Although the contribution of the title reaction to ethenol formation is not significant for the studied cyclohexane flame, it might contribute more in the case where the concentration of propene is more significant, such as in propene flames. Ethenol mole fraction was measured to be on the order of 10^{-4} in a rich propene premixed flame,[8] and more detailed future data would provide a test of the potential role of OH + propene.

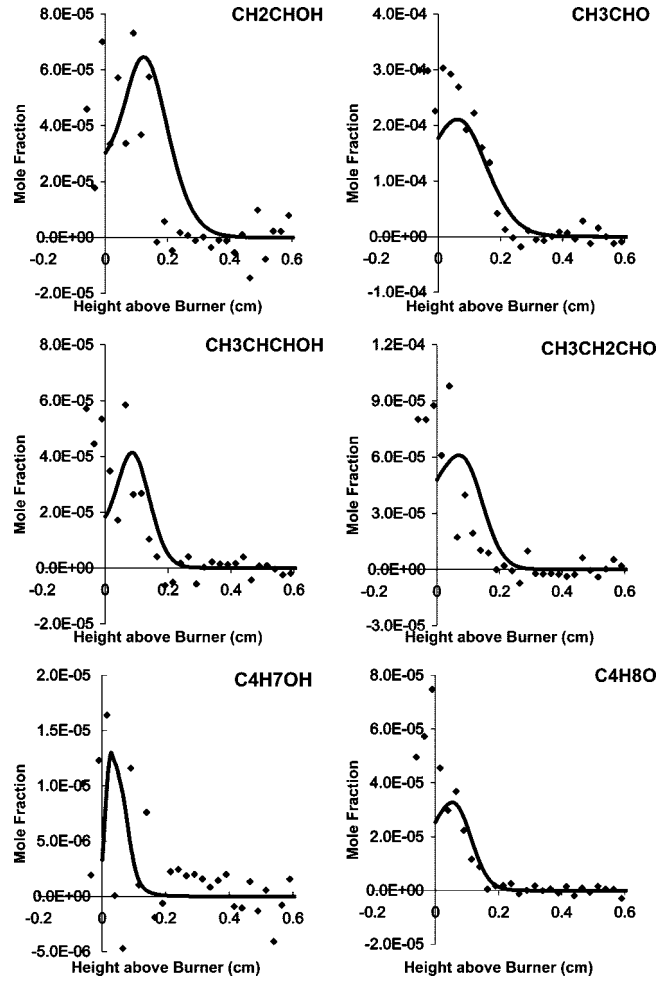

Figure 8. The predicted and measured concentration profiles of enols, aldehydes in a cyclohexane premixed flame. Solid symbols represent the experimental data (ref [29]), while lines represent the simulations.

VI. Conclusion

A complete PES for OH addition to propene was mapped at the CCSD(T)/cc-pVDZ//B3LYP/cc-pVTZ level of theory. The rate constants of different product channels and branching ratios were calculated using the Master Equation formulation. It was found that ethenol formation is the dominant pathway for the addition reactions to form bimolecular products. Propenol was also formed but with a much smaller concentration. It was found that in the temperature range considered, hydrogen abstraction is more significant than addition reactions in the overall rate with a branching ratio of more than 90%.

The calculated rate constants for ethenol and propenol formation were included in the Utah Surrogate Mechanism to model the enol profile in a cyclohexane premixed flame. The extended model shows some consistency with the experimental data. Further analysis shows that although the contribution of ethenol formation from OH + propene reaction is small (5%) in this flame, its role expected to be significant when the concentration of the reactant (propene) is large.

Acknowledgment. This work is supported in part by the National Science Foundation to T. N. Truong. L.K.H. is grateful to the Vietnam Education Foundation for a Graduate Fellowship. An allocation of computer time from the Center for High Performance Computing at the University of Utah is gratefully acknowledged. The computational resources for this project have been provided by the National Institutes of Health (Grant # NCRR 1 S10 RR17214-01) on the Arches Meta-cluster, administered by the University of Utah Center for High-Performance Computing. Work by M.E.L. and P.R.W. is supported by the Office of Basic Energy Sciences (BES), U.S. Department of Energy (USDOE), under DE-FG02-91ER14192, and certain of the flame measurements were conducted in their collaboration at the Advanced Light Source of Lawrence Berkeley National Laboratory with T. A. Cool, N. Hansen, K. Kohse-Höinghaus, and co-workers.

Supporting Information Available: Cartesian coordinates and frequencies of reactants, isomers, saddle-points, and products at the B3LYP/cc-pVTZ. This material is available free of charge via the Internet at http://pubs.acs.org.

References and Notes

(1) Benioff, M. R.; Lazowska, E. D.; Bajcsy, R.; Hannigan, W. J.; Jr., J. C. B.; Javitt, J. C.; Celis, P.; Klavans, J. L.; Evans, P. T.; Leighton, F. T.; Fernandez, M. A.; Fiallo, L. E.; Mortazavian, H.; Griffiths, J.-M.; Mott, R. D.; Neupert, P. M.; Noam, E. M.; Patterson, D. A.; Quintanilla, A. G.; Reed, D. A.; Spafford, E. H.; Staelin, D. H.; Tippett, P. S.; Yang, G.; Reed, D. A.; Bajcsy, R.; Fernandez, M. A.; Griffiths, J.-M.; Mott, R. D.; Dongarra, J.; Johnson, C. R. Report to the President - Computational Science: Ensuring America's Competitiveness, 2005.

(2) Miller, J. A.; Pilling, M. J.; Troe, J. *Proc. Combust. Inst.* **2005**, *30*, 43.

(3) Naidja, A.; Krishna, C. R.; Butcher, T.; Mahajan, D. *Prog. Energy Combust. Sci.* **2003**, *29*, 155.

(4) Walters, K. M.; Dean, A. M.; Zhua, H.; Kee, R. J. *J. Power Sources* **2003**, *123*, 182.

(5) Sullivan, P. A.; Ploeger, J. M.; green, W. H.; Tester, J. W. *Phys. Chem. Chem. Phys.* **2004**, *6*, 4310.

(6) Ricca, A.; Bauschlicher, C. W., Jr.; Bakes, E. L. O. *Icarus* **2001**, *154*, 516.

(7) Taatjes, C. A.; Hansen, N.; McIlroy, A.; Miller, J. A.; Senosiain, J. P.; Klippenstein, S. J.; Qi, F.; Sheng, L.; Zhang, Y.; Cool, T. A.; Wang, J.; Westmoreland, P. R.; Law, M. E.; Kasper, T.; Kohse-Höinghaus, K. *Science* **2005**, *308*, 1887.

(8) Taatjes, C. A.; Hansen, N.; Miller, J. A.; Cool, T. A.; Wang, J.; Westmoreland, P. R.; Law, M. E.; Kasper, T.; Kohse-Hoinghaus, K. *J. Phys. Chem. A* **2006**, *110*, 3254.

(9) Senosiain, J. P.; Klippenstein, S. J.; Miller, J. A. *J. Phys. Chem. A* **2006**, *110*, 6960.

(10) Miller, J. A.; Klippenstein, S. J. *J. Phys. Chem. A* **2006**, *110*, 10528.

(11) Holbrook, K. A.; Pilling, M. J.; Robertson, S. H. *Unimolecular Reactions*; Wiley: New York, 1996.

(12) Gilbert, R. G.; Smith, S. C. *Theory of Unimolecular and Recombination Reactions*; Blackwell: Oxford, 1990.

(13) Becke, A. D. *Phys. Rev. A* **1988**, *38*, 3098.

(14) Woon, D. E.; Dunning, T. H., Jr. *J. Chem. Phys.* **1993**, *98*, 1358.

(15) Gonzalez, C.; Schlegel, H. B. *J. Chem. Phys.* **1989**, *90*, 2154.

(16) Becke, A. D. *J. Chem. Phys.* **1993**, *98*, 1372.

(17) Lee, C.; Yang, W.; Parr, R. G. *Phys. Rev.* **1988**, *37*, 785.

(18) Truong, T. N. *J. Chem. Phys.* **1994**, *100*, 14.

(19) Truong, T. N.; Duncan, W. *J. Chem. Phys.* **1994**, *101*, 7408.

(20) Lynch, B. J.; Fast, P. L.; Harris, M.; Truhlar, D. G. *J. Phys. Chem. A* **2000**, *104*, 4811.

(21) Szori, M.; Fittschen, C.; Csizmadia, I. G.; Viskolcz, B. *J. Chem. Theory Comput.* **2006**, *2*, 1575.

(22) Zhang, Q.; Bell, R.; Truong, T. N. *J. Phys. Chem.* **1995**, *99*, 592.

(23) Frisch, M. J.; Trucks, G. W.; Schlegel, H. B.; Scuseria, G. E.; Robb, M. A.; Cheeseman, J. R.; Montgomery, J. A.; Jr.; , T. V.; Kudin, K. N.; Burant, J. C.; Millam, J. M.; Iyengar, S. S.; Tomasi, J.; Barone, V.; Mennucci, B.; Cossi, M.; Scalmani, G.; Rega, N.; Petersson, G. A.; Nakatsuji, H.; Hada, M.; Ehara, M.; Toyota, K.; Fukuda, R.; Hasegawa, J.; Ishida, M.; Nakajima, T.; Honda, Y.; Kitao, O.; Nakai, H.; Klene, M.; Li, X.; Knox, J. E.; Hratchian, H. P.; Cross, J. B.; Adamo, C.; Jaramillo, J.; Gomperts, R.; Stratmann, R. E.; Yazyev, O.; Austin, A. J.; Cammi, R.; Pomelli, C.; Ochterski, J. W.; Ayala, P. Y.; Morokuma, K.; Voth, G. A.; Salvador, P.; Dannenberg, J. J.; Zakrzewski, V. G.; Dapprich, S.; Daniels, A. D.; Strain, M. C.; Farkas, O.; Malick, D. K.; Rabuck, A. D.; Raghavachari, K.; Foresman, J. B.; Ortiz, J. V.; Cui, Q.; Baboul, A. G.; Clifford, S.; Cioslowski, J.; Stefanov, B. B.; Liu, G.; Liashenko, A.; Piskorz, P.; Komaromi, I.; Martin, R. L.; Fox, D. J.; Keith, T.; Al-Laham, M. A.; Peng, C. Y.; Nanayakkara, A.; Challacombe, M.; Gill, P. M. W.; Johnson, B.; Chen, W.; Wong, M. W.; Gonzalez, C.; Pople, J. A., *Gaussian 03, Revision A.1*; Gaussian, Inc.: Wallingford, CT, 2003.

(24) Miller, J. A.; Klippenstein, S. J.; Robertson, S. H. *J. Phys. Chem. A* **2000**, *104*, 7525.

(25) Huynh, L. K.; Zhang, S.; Kungwan, N.; Truong, T. N. In preparation.

(26) Troe, J. *J. Chem. Phys.* **1977**, *66*, 4745.

(27) Reid, R. C.; Prausnitz, J. M.; Sherwood, T. K. *The Properties of Gases and Liquids*, 3rd ed.; McGraw-Hill: New York, 1977.

(28) Forst, W. *Theory of Unimolecular Reactions*; Academic Press: New York, 1973.

(29) Law, M. E.; Westmoreland, P. R.; Cool, T. A.; Wang, J.; Taatjes, C. A.; Hansen, N.; Kasper, T. Proc. 4th Joint Meeting of the US Sections of the Combustion Institute 2005.

(30) Miller, J. A.; Chandler, D. W. *J. Chem. Phys.* **1986**, *85*, 4502.

(31) Chandler, D. W.; Millam, J. M. *J. Chem. Phys.* **1984**, *81*, 445.

(32) Miller, J. A.; Klippenstein, S. J. *J. Phys. Chem. A* **2001**, *105*, 7254.

(33) Curran, H. J.; Gaffuri, P.; Pitz, W. J.; Westbrook, C. K. *Combust. Flame* **2002**, *129*, 253.

(34) Greenwald, E. E.; Park, J.; Anderson, K. C.; Kim, H.; Reich, B. J. E.; Miller, S. A.; Zhang, R.; North, S. W. *J. Phys. Chem. A* **2005**, *109*, 7915.

(35) Glasstone, S.; Laidler, K. J.; Eyring, H. *The Theory of Rate Processes*; McGraw-Hill: New York, 1941.

(36) Miller, W. H. *J. Am. Chem. Soc.* **1979**, *101*, 6810.

(37) Truong, T. N.; Nayak, M.; Huynh, H. H.; Cook, T.; Mahajan, P.; Tran, L.-T. T.; Bharath, J.; Jain, S.; Pham, H. B.; Boonyasiriwat, C.; Nguyen, N.; Andersen, E.; Kim, Y.; Choe, S.; Choi, J.; Cheatham, T. E., III.; Facelli, J. C. *J. Chem. Inf. Model.* **2006**, *46*, 971.

(38) Kee, R. J.; Rupley, F. M.; Miller, J. A.; Coltrin, M. E.; Grcar, J. F.; Meeks, E.; Moffat, H. K.; Lutz, A. E. Dixon-Lewis, G.; Smooke, M. D.; Warnatz, J.; Evans, G. H.; Larson, R. S.; Mitchell, R. E.; Petzold, L. R.; Reynolds, W. C.; Caracotsios, M.; Stewart, W. E.; Glarborg, P.; Wang, C.; Adigun, O.; Houf, W. G.; Chou, C. P.; Miller, S. F.; Ho, P.; Yang, D. J., *Chemkin Collection, Release 4.0*; Reaction Design, Inc.: San Diego, CA, 2004.

(39) Zhang, H. R.; Eddings, E. G.; Sarofim, A. F. *Combust. Sci. Technol.* **2007**, *179*, 61.

(40) Zhang, H. R.; Huynh, L. K.; Kungwan, N.; Yang, Z.; Zhang, S. *J. Phys. Chem. A* **2007**, *111*, 4102.

(41) Tsang, W. *J. Phys. Chem. Ref. Data* **1991**, *20*, 221.

(42) Hoyermann, K.; Sievert, R. *Ber. Bunsen-Ges. Phys. Chem.* **1979**, *83*, 933.

(43) Smith, G. P.; Fairchild, P. W.; Jeffries, J. B.; Crosley, D. R. *J. Phys. Chem.* **1985**, *89*, 1269.

(44) Tully, F. P.; Goldsmith, J. E. M. *Chem. Phys. Lett.* **1985**, *116*, 345.

(45) Bott, J. F.; Cohen, N. *Int. J. Chem. Kinet.* **1991**, *23*, 1075.

(46) Yetter, R. A.; Dryer, F. L. *Proc. Combust. Inst.* **1992**, *24*, 757.

(47) Warnatz, J. *Rate coefficients in the C/H/O system. In Combustion Chemistry*;. Gardiner, W. C., Jr., Ed.; Springer-Verlag: New York, 1984.

JP808050J